Fusion Engineering and Design 167 (2021) 112343

Contents lists available at ScienceDirect

Fusion Engineering and Design

journal homepage: www.elsevier.com/locate/fusengdes

Design optimization of the Upper Steering Mirror Assembly (USMA) for ITER ECHUL in view of disruptive events

Matteo Vagnoni *, René Chavan, Timothy Goodman, Anastasia Xydou

École polytechnique fédérale de Lausanne, Swiss Plasma Center, CH-1015, Lausanne, Switzerland

ARTICLE INFO

Keywords:
ITER
EC UL
Thermo-mechanical analysis
Cooling system

ABSTRACT

Four Electron Cyclotron Heating Upper Launchers (ECHUL) will be used at ITER to counteract magneto-hydrodynamic plasma instabilities by targeting them with up to 20 MW of mm-wave power at 170 GHz. The millimeter waves are guided through a set of fixed mirrors (M1, M2 and M3) and the front steering mirror set (M4), aiming at the correct location in the plasma for suppression of the q = 3/2 and q = 2/1 Neoclassical Tearing Modes (NTMs). At the M4 reflecting mirror surfaces, part of the mm-wave power is converted into heat by ohmic dissipation, totaling ca. 25 kW of absorbed power and reaching a peak power density of up to 1.8 MW/m^2 in each of the 4 beam center spots.

The latest in-vessel mm-wave mirrors Components Load Specification (CLS) data imposes an increase of the electromagnetically induced loads relative to those anticipated in earlier designs, resulting in higher mechanical load on the Crossed Flexure Pivot (CFP) due to Vertical Displacements Events (VDEs). The present paper reports the main design optimizations as well as the finite elements analyses carried out with the objective to: 1) reduce the electromagnetic loads on the components due to induced Eddy currents, 2) dissipate the thermal loads coming from the beams themselves and the plasma following the design requirements in terms of coolant temperature rise, pressure drop and admissible corrosion rate values, 3) assure the components structural integrity enforcing the ITER Structural Design Code for the In-Vessel Components (SDC-IC).

1. Introduction and background

The four ITER ECHUL feature eight transmission lines (TLs) that are used to inject microwave power up to 1.31 MW per line at 170 GHZ (Fig. 1) at chosen rational magnetic flux surfaces in order to stabilize NTMs. The mm-waves are guided through a quasi-optical configuration, in which four beams are incident per mirror, passing via a set (upper and lower) of three fixed mirrors (M1, M2, and M3) until reaching the front steering mirrors M4, which aim at the correct location in the plasma.

Consolidated in 2019 for the normal operation scenario [1,2], two steering mirrors M4 consist of a frictionless mechanism actuated by helium. Stator, rotor, four bellows and six elastic springs are mutually connected through a pair of Crossed Flexure Pivots (CFP) enabling 14° of rotation of the reflective mirror, which is ultimately bolted to the rotor (Fig. 2). Because of their location in the UL front-end region they are subject to severe operating conditions. Firstly, the M4 components are exposed to a significant nuclear heating (peak of 1.5 MW/m^3) and thermal heat flux due to their direct line of sight into the plasma. Secondly, the ohmic loss produced at the 2 mm thick copper alloy reflector generates circa 30 kW of power that must be dissipated through an embedded cooling circuit. Finally, transient disruptive scenarios like Vertical Displacement Events (VDE) may suddenly occur, resulting in loading conditions more severe than the one anticipated in the previous design phase specially, on any thin membrane such as the one used for the CFP. Due to the evolving ITER requirements, an optimization of the Upper Steering Mirror 4 (USM4) is being carried out to make the design compliant to disruptive scenarios.

Identified as design driver, the load case ID 6 is selected from the latest Component Load Specification (CLS, [3]). It corresponds to a situation where the antenna is being used to reflect mm-wave power from M4, when a vertical displacement event type II (the type describes the severity) and a seismic type 1 (SL1) event occur. This scenario is initiated by a seismic event, then a loss of vertical control arises where the plasma shifts upward or downwards while maintaining its current. A thermal quench finally occurs during the vertical drift, followed by a subsequent current quench [4]. Significant Eddy currents are induced in the steering mirror components that are partially made of highly electrically-conductive copper alloy. Consequently, the interaction

* Corresponding author.
E-mail address: matteo.vagnoni@epfl.ch (M. Vagnoni).

https://doi.org/10.1016/j.fusengdes.2021.112343
Received 26 November 2020; Received in revised form 8 February 2021; Accepted 11 February 2021
Available online 20 February 2021

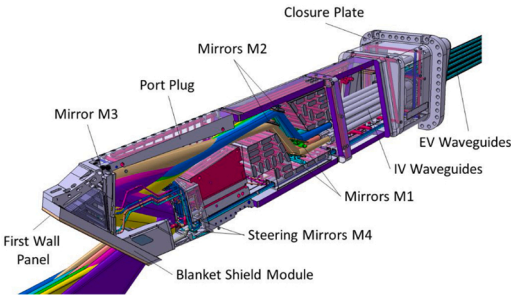

Fig. 1. ITER Electron Cyclotron Heating Upper Launcher.

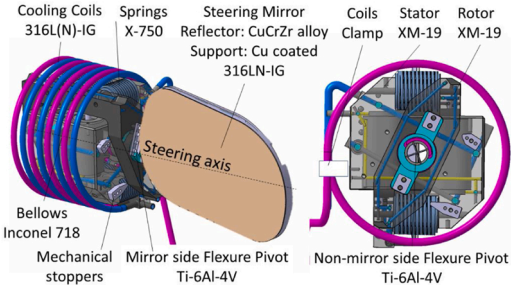

Fig. 2. Upper Steering Mirror Assembly (USMA), 2 mm Cu alloy, 100 % reflecting surface coverage (yr. 2019). The asymmetric shape of the mirror (relative to the rotation axis) corresponds to the contour of the reflected beams with a beam size factor of 1.5.

between external magnetic fields and induced currents generates significant moments and forces. Fig. 3 shows the time line of the moment around "Z" during the VDEII when a peak value of 0.5 kN m is reached, of which 70 % is contributed by the 2mm-thickness CuCrZr alloy reflector required for minimizing the ohmic losses, increase the transverse heat diffusion and optimize the heat removal through the cooling system.

Within the USM4 assembly, the titanium alloy CFPs are the components with the highest mechanical stress. Preliminary stress analysis has shown that the von Mises stress in the blades of the mirror CFP (peak of 959.5 MPa) reaches values beyond the elastic limit (547 MPa at 250 °C, [6]).

This paper reports the analyses carried out to support the design optimization. Firstly, a parametric structural analysis investigates on the reduction of the generated EM load to reduce the blade's stress to an acceptable level. Secondly, a parametric EM analysis shows the correlation between the Cu alloy content and induced moment at the mirror/rotor sub-model. Finally, these findings are used to finalize the UM4 design which is thermo-mechanically verified against the SDC-IC code [7].

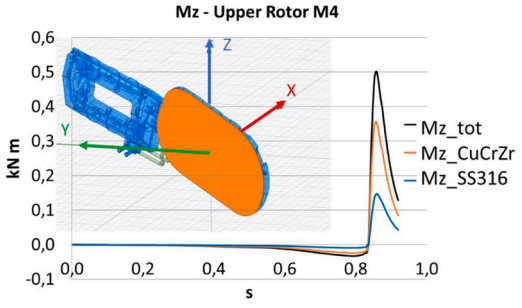

Fig. 3. Time history of the electromagnetic load on Upper M4 mirror and rotor due to the VDEII event, in the configuration with the 2mm-thickness CuCrZr alloy reflector bonded to stainless steel support (yr. 2019 design, [5]).

2. Parametric structural analysis

A parametric structural elastic analysis is performed in ANSYS workbench 2019R3 [8] in order to quantify the required EM load reduction. The stress illustrated in Fig. 4 is the result of the simultaneous application of the Normal Operation (NO), the seismic inertial load (SL1) and the VDII load (the peak value is applied as a static value). The latter is parametrized and linearly scaled down from 100 % of its magnitude to 50 % repeating the same type of analysis 6 times. The mirror side CFP stress evolution is then plotted versus the load showing the required reduction.

2.1. Numerical model and boundary conditions

The CAD model of the USM4, 2019 design (Fig. 3) is extracted from the ITER database and used for the mesh creation. The following parameters and modifications are applied:

1 The bolts and alignment pins are not part of the assessment. The surfaces in contact are meshed as continuous bodies.
2 Linear elastic material properties are used.
3 Mechanical stoppers are simulated through frictionless contact rotor-stopper as the VDEII load might move the rotor to one of the two extremes.
4 Four bellows simplified modelling only the core (no membrane). The equivalent stiffness equal to 10,105 N/m is applied via spring elements.
5 1.44E6 quadratic elements solid 186–187 are used to mesh the components.
6 The displacements of the stator' surface in contact with the supporting frame are set to zero in all directions. In parallel, cooling coils displacements of the endings (in proximity of the clamps) are set to zero.

The following table summarizes the loads completing the finite element model.

2.2. Results

The investigated scenario is defined as a Cat. II event according to [3]. This means that the following plastic collapse criteria has to be satisfied for the CFP:

$$\overline{P_L + P_b} \leq K_{eff} S_m(T_m \Phi t_m) \quad (1)$$

where:

P_L= local primary membrane stress tensor
P_b= Primary bending stress tensor
$\overline{P_L + P_b}$= Stress intensity of the sum of the tensor P_L and P_b
K_{eff}= an effective bending shape factor
S_m= Allowable stress for the thickness-averaged temperature and neutron fluence calculated along the supporting line segment.

Four Stress Classification Lines (SCLs) are generated through the blades thickness at the shell-blade junction, that being the most stressed

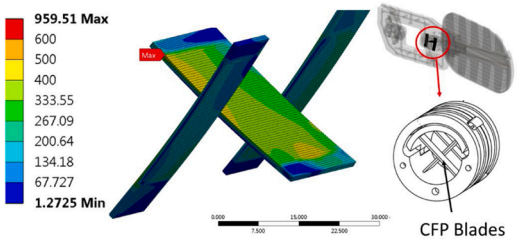

Fig. 4. Blades von Mises stress for the mirror side CFP.

region. The allowable ($K_{eff}S_m$) for the Ti alloy equals to 337 MPa, [6].

Fig. 5 shows that the magnitude of VDEII structural forces and moments have to be reduced by 30 % for the Ti alloy to pass the plastic collapse check. In order to cover other failure modes in other scenarios - e.g. fatigue - the load reduction is targeted to 50 %.

3. Parametric electromagnetic analysis

The usual ITER methodology recommends to create a model using a 20° sector of the vacuum vessel that includes blanked modules, upper and equatorial ports, and portions of the magnets and the plasma in which to apply poloidal and toroidal time-dependant values of the currents [9]. However, given the size of the model, such an approach requires considerable computational resources; resulting in the limitation that a detailed geometry of UM4 cannot be used.

Two parametric transient electromagnetic analyses have been carried out using ANSYS Maxwell R3 [8] in order to evaluate the induced forces and moments occurring in the USM4 rotor and mirror, for the VDEII case, with respect to the: 1) variation of the Cu alloy thickness; 2) variation of Cu alloy surface coverage. The sub-modelling procedure is applied [10] to account for the detailed geometry variations.

3.1. Numerical model and boundary conditions

3.1.1. Geometry and mesh

The geometry of the USM4 rotor and mirror is taken from the Finite Element Model (FEM) developed for §2. Two concentric spheres with a radius of 1.5 and 8 m are modelled to simulate the vacuum boundary (different mesh size is applied).

The Cu alloy reflector coverage has been parametrized with respect to the dimension "ax", Fig. 6. Nine design points are computed, setting the "ax" dimension from 155 to 75 mm, with steps of 10 mm. Such copper reduction towards the centre of the mirror entails the replacement of the outer region with SS material (blue ring, Fig. 6). The rational is given by the fact that Ohmic loss heat flux due to mm wave propagation has the highest peaks (four) in the centre region of the mirror (§4). In this way, the thermal heat sink will keep its function at this location, while minimizing Eddy currents in the outer region.

In a second step, the thickness of the Cu alloy reflector is parametrized changing it from 2 to 0.5 mm, with steps of 0.25 mm and keeping the full Cu alloy surface coverage.

Mesh settings and material properties are reported below:

3.1.2. Excitations

Three pairs of Helmholtz coils have been drawn to reproduce the magnetic field components B_x, B_y, B_z, (Fig. 7). This type of excitation allows to model a variation of magnetic field which is nearly uniform at the centre of the pair of coils. The directional magnetic flux density is extracted from [5], and converted to current using the following expression:

$$I = \left(\frac{5}{4}\right)^{3/2} \frac{\vec{B}r}{\mu_0} \tag{2}$$

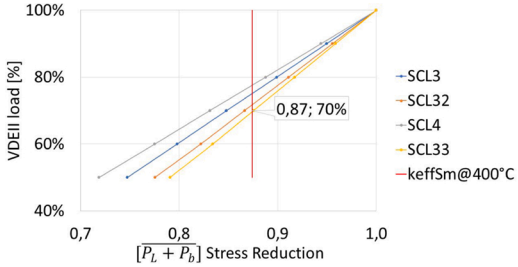

Fig. 5. CFP stress evolution Vs load reduction.

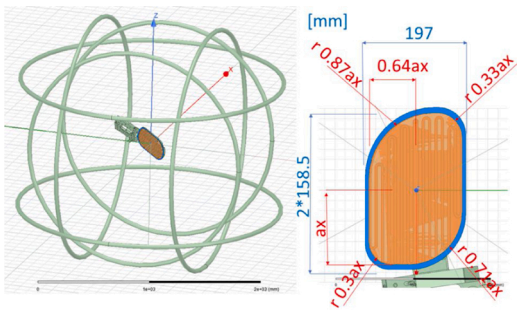

Fig. 6. EM Maxwell model with the Helmholtz coils (left), main dimensions and ratios of the UM4 Cu alloy surface coverage parametrization (right), where the coefficient on the radius expresses the ratio of copper to steel surface.

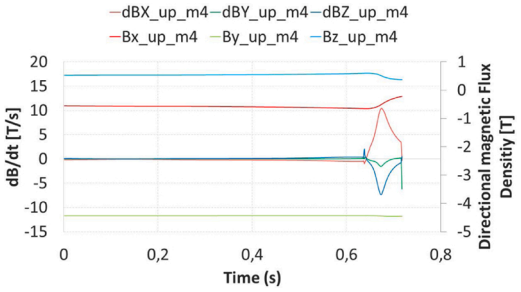

Fig. 7. Time history of the magnetic field [T] in X, Y, Z directions and variation of field [T/s] for the VDEII linear case at the center of the UM4 reflecting surface.

where:

μ_0 = permeability of free space ($4\pi \cdot 10^{-7}\ T \cdot m/A$)
I = coil current (A)
r = coil radius (m)

3.2. Results

The current density plot shows the highest magnitude occurring in the Cu alloy reflector at the time 0.676 s when the peak of dB/dt is reached (Fig. 8).

As a consequence, currents aligned with the Z direction couple with the nearly constant toroidal magnetic field, By, generating force density vectors at the top-right and bottom left of the mirror, Fig. 9.

Their vectoral summation translates into a non-negligible USM4 Mz moment which is the design driver. Fig. 10 shows that M_z_Cu torque non-linearly reduces as the parameter "ax" diminishes.

Alternately, Fig. 11 indicates that torque Mz_Cu linearly decreases with the reduction of Cu-alloy thickness.

The results illustrated in Figs. 10 and 11 are used to meet the

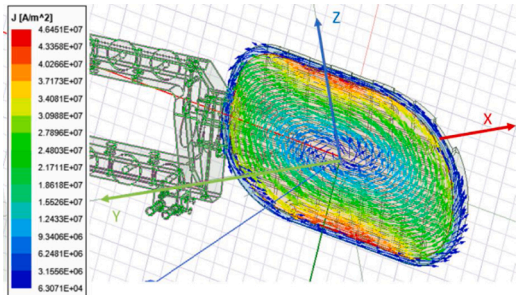

Fig. 8. Current density [A/m^2] for the time instant t = 0.676 s for ax = 145 mm.

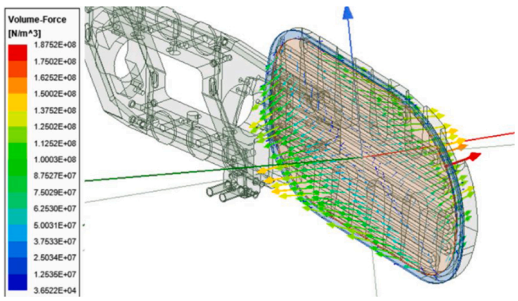

Fig. 9. Force density [N/m^3] for the time instant t = 0.676 s for ax = 145 mm.

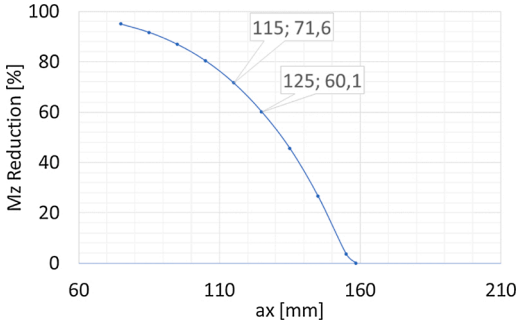

Fig. 10. Mz_Cu torque reduction [%] as function of the parameter "ax" [mm] for the 2 mm constant thickness of the Cu alloy reflector.

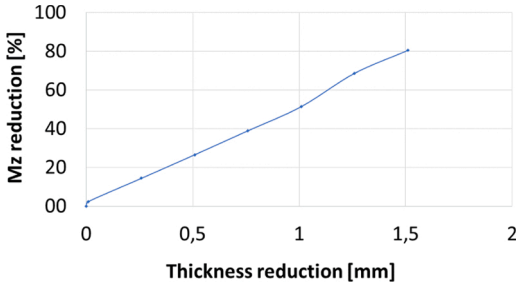

Fig. 11. Mz_Cu torque reduction as function of the Cu alloy thickness reduction.

objective of 50 % reduction of the VDEII EM loads. With reference to Fig. 3, such moment reduction is achievable setting the "ax" dimension to 115 mm while keeping the 2 mm thickness of the Cu alloy reflector. This means a reduction of the Cu-alloy induced torque of circa 71.6 %, meaning a new total USM4 Mz torque of 253 Nm. All possible design points are the Boundary Conditions (BC) for the next parametric thermo-mechanical analysis, since any reduction of Cu-alloy is expected to modify the cooling efficiency increasing the thermal gradient of the reflector.

4. Parametric thermal-mechanical analysis of the UM4 mirror

The modification of the CuCrZr-SS ratio at the reflecting region modifies the way the ohmic loss power is dissipated through the water-cooling system. The SMA is cooled with PHTS water routed through pipes independent from the port plug cooling, with a manifold system located at the port plug closure plate. A parametric thermal-mechanical analysis is carried out with ANSYS 2019R3 [8] to assess the temperature fields occurring at the Cu reflector and SS support for the steady state case. Afterwards, these fields are used as boundary condition for the static elastic structural analysis to evaluate stress and strain taking place at the USM4. Such procedure is repeated for different Design Points (DPs) with the single objective to minimize the stress at the SS316L(N) USM4 region.

4.1. Geometry and parameters

The geometry of the mirror is taken from upstream analyses and key geometric parameters (Fig. 12) are scanned between the two boundary values given in the CLS [3] and resulting from upstream analyses (Tables 1–3).

The Cu alloy thickness (Cu_TK) dimension, initially set to 2 mm and already optimized in size (ax = 115 mm, fixed), can only decrease to reduce the EM load (Fig. 11). At the same time, such thickness should not be reduced too much to act as a heat sink. Its lower bound is set to 1 mm.

The size of the stainless-steel top layer (Ch_top_TK) cannot be suppressed as the water must remain within SS walls due to erosion/corrosion phenomena otherwise arising when in contact with Cu alloy walls. On the other hand, a significant thickness would act as thermal barrier, with poor thermal transfer, due to the SS thermal conductivity. A preliminary manufacturability assessment recommends not to reduce this dimension below 1 mm. The same rationale is used to define the lateral channel thickness (Ch_lateral_TK). The dimensions of the water-cooling channel height and width are determined by the preliminary estimated HTC, and ultimately to the allocated mass flow. As a consequence, the cross-section area should not exceed a value of 28 mm^2.

4.2. Material properties

Linear elastic material properties of the CuCrZr alloy and SS316 L(N) are selected for the structural part of the analysis. Temperature-dependent properties are used for the steady-state analysis (Figs. 13 and 14).

4.3. Boundary conditions

The following boundary conditions relative to the normal operation scenario are extracted from the CLS [3] and used for the thermal part of the analysis:

- Constant volumetric heating of 0.5374 MW/m^3 totaling circa 0.5 kW of deposited power
- Constant heat flux of 9700 W/m^2 due to stray power applied on the back-mirror surfaces totaling 0.7 kW of power
- Ohmic loss heat flux is obtained through quasi optical beam analysis [11] and applied using CuCrZr electric resistivity at 250 °C and "S" factor of 2.2. it accounts for circa 22 kW of power deposition.
- During the plasma burn phase, the reflecting surface is exposed to a peak heat flux of 57 kW/m^2 totaling 3.2 kW of power deposition.
- A Heat Transfer Coefficient (HTC) of 55 kW/m^{2}K with a bulk temperature of 100 °C (mean temperature of cooling water between inlet and outlet) is initially applied to the cooling channel serpentine

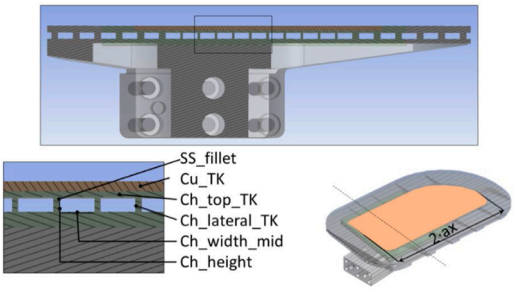

Fig. 12. UM4 mirror cross section (top), geometric parameters for the cooling optimization (bottom-left) and size of the copper heat sink (bottom-right).

Table 1
Loads Vs Ansys Time steps.

Loads	Time steps				
	1	2	3	4	5
Spring preload (mm)	17.4	17.4	17.4	17.4	17.4
Bellow Pressure (MPa)	0	2	2	2	2
VDEII loads	–	–	ON	ON	ON
SL1 & Gravity accelerations (m/s^2)	–	–	–	$a_x = 19.4$ $a_y = 5.1$ $a_z = 51.4$	
Temp. fields mapped on components due NO	–	–	–	–	ON

Table 2
Mesh and material properties.

	Coils	Mirror	Support	Inner sphere	Outer sphere
Element min. size [m]	0.01	0.0005	0.01	0.3	1.5
Material	Cu	CuCrZr alloy	316LN	vacuum	vacuum
Elect. Conductivity (S/m)		4.6E7	1.3E6	–	–

Table 3
Geometrical parameters.

Parameters [mm]	Initial value	Lower bound	Upper bound
Cu_TK	2	0.9	2
Ch_top_TK	1	0.9	1.5
Ch_lateral_TK	1	0.7	1
Ch width	7	3	7
Ch_height	4	2	4
S_fillet	0.8	–	–

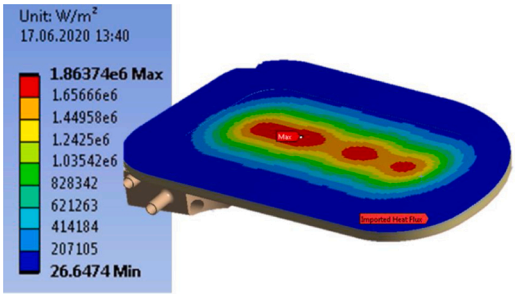

Fig. 13. Gaussian ohmic loss heat flux distribution on the UM4 reflecting surface.

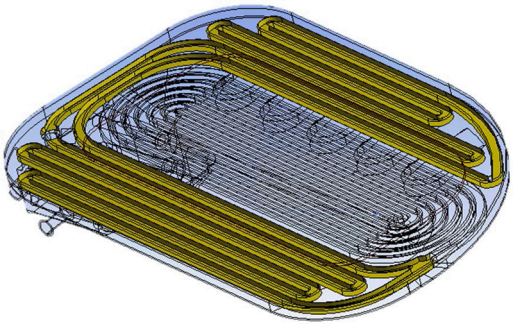

Fig. 14. UM4 cooling flow after the bifurcation, HTC = 27,500 W/m2K.

below the Cu heatsink. After flowing through the center channel, the water flow bifurcates towards the less-thermally-loaded portion of the mirror, where the HTC value is half of the center serpentine as the width of the cross-section doubles in size. Finally, during the optimization, the HTC is swept from 45,000 to 60,000 W/m^{2}K. The upper bond is estimated using the max. channel cross-section (28 mm^2) and the max. allocated flow of 0.21 kg/s.

The structural part of the analysis uses the following BCs:

- Temperature fields coming from the above-mentioned analysis, with an initial temperature of 80 °C (inlet temp. of the cooling water)
- Dx, Dy, Dz displacements of the faces of the bolted joint are set to zero
- Gauge pressure of 4.4 MPa is applied to the cooling walls

4.4. Results of parametric analysis

The parameters are plotted against the von Mises stress occurring at the SS part of the mirror to visualize the dependencies and select the optimal design point. The example in Fig. 15 shows that the stress at the interface Cu-SS diminishes to 300 MPa while increasing the Cu thickness to 2 mm. This is because the strong thermal gradient across the thickness (from reflecting surface, downward) is better distributed laterally homogenizing the temp. at the interface. This translates into a lower stress.

Similarly, the same type of tradeoff is repeated for the different parameters creating the Table 4.

The study shows that the channel cross-section of H6xW4 mm with 2 mm Cu alloy thickness guarantees an optimal stress state of the heatsink and SS pressure vessel. This occurs imposing a minimum cooling wall thickness of 1 mm.

4.5. Thermal results

The temperature plot of the UM4 is reported in Fig. 16. As expected, the strongest temperature gradient occurs at the 3-mm-thickness region comprised by the reflecting surface (258 °C) and the cooling channel (≈140 °C).

The rest of the mirror structure reaches an average temp of 100−150 °C especially at the outer region of the UM4

4.6. Structural results

Fig. 17 shows the final stress state of the UM4 SS part that includes Primary (P) and secondary (Q) stress. Von Mises stress of 377 MPa is reached at the interface with the CuCrZr alloy heat sink. Such region will be further investigated applying the SDC-IC [7] code. While the back part of the SS support works under a moderate stress state of circa

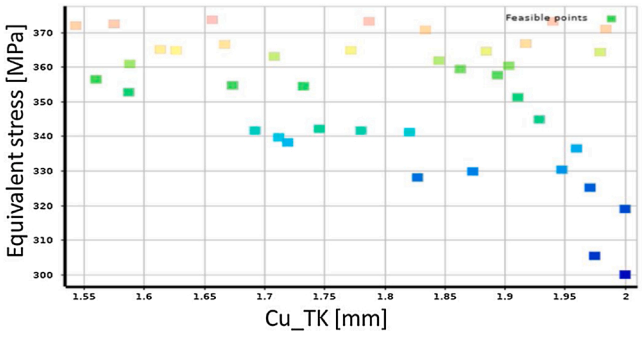

Fig. 15. Cu heatsink thickness [mm] versus equivalent SS stress [MPa] - blue = feasible DPs, green = less feasible DPs, red = not recommendable DPs (For interpretation of the references to colour in this figure legend, the reader is referred to the web version of this article).

Table 4
List of potential design points.

Cu_TK [mm]	Ch top wall [mm]	Ch width [mm]	Ch height [mm]	Ch lateral wall [mm]	Stress SS [MPa]	Stress Cu [MPa]
2	1	7	4	1	429.4	259.6
2	1	8	3	1	423.6	281.2
2	1	6	4	1	362.1	258.1
2	1	5	4	1	369.6	262.5
2	1	5	3	1	396.6	281.2
2	1	8	2	1	427.5	305.8
1	1	6	4	1	433.2	314.6

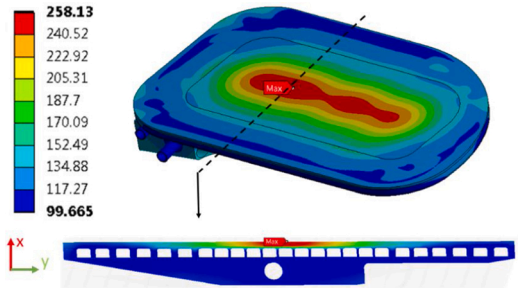

Fig. 16. Temperature gradient [°C] of the UM4 and the most loaded section.

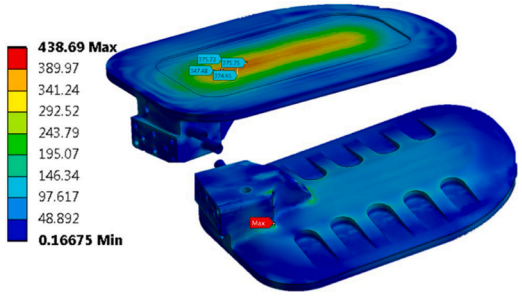

Fig. 17. P + Q stress of the SS vessel [MPa].

130−150 MPa, a numerical singularity appears at the sharp corner of the bolted joint (439 MPa). The final state of the Cu alloy heatsink is also post-processed showing a peak von Mises value of 266 MPa.

SDC-IC [7] is enforced to verify the integrity of the vessel under the NO scenario. SCLs (Fig. 18) are generated at the region of interest (Cu-SS interface at the peak stress/ temperature) in order to decouple P and Q stresses.

Table 5 shows that the SS316LN-IG pressure vessel primary and secondary stresses are within the material limit.

The fatigue failure mode is also checked for the SS pressure vessel calculating the strain range as:

$$\overline{\Delta\varepsilon} = \overline{\Delta\varepsilon}_1 + \overline{\Delta\varepsilon}_2 + \overline{\Delta\varepsilon}_3 + \overline{\Delta\varepsilon}_4 \quad (3)$$

Where:

$\overline{\Delta\varepsilon}_1 = \frac{2}{3}(1+\nu)(\overline{\Delta\sigma_{tot}/E})$, strain given by the elastic analysis;

$\overline{\Delta\varepsilon}_2$ is the plastic strain induced by cyclic primary stress;

$\overline{\Delta\varepsilon}_3$ is the amplification of plastic strain due to elastic follow-up;

$\overline{\Delta\varepsilon}_4$ is the amplification of plastic strain due to multi-axial Poisson's effect.

Table 6 shows that the usage factor is equal to 0.86 and satisfies the mirror functional required cycles.

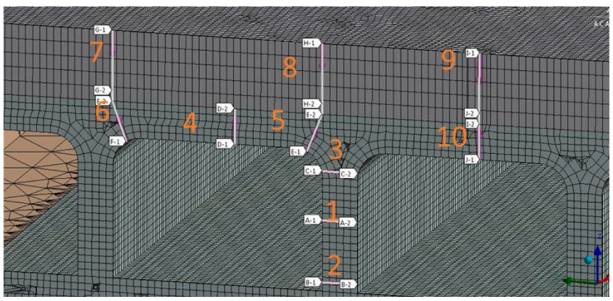

Fig. 18. SCLs lines.

Table 5
Structural integrity verification of SS316LN-IG.

Design criteria	SCLs						
	1	2	3	5	6	7	**Limit**
Pm	27	–	–	–	–	3.6	121
Pl + Pb	–	24.7	26	19	19	–	181.5
Pl + Pb + Q	–	201	162	–	–	214	243

Table 6
Summary of fatigue check for the SS part of the UM4.

Temp [°C]	$\Delta\sigma_{tot}$ [MPa]	$\overline{\Delta\varepsilon}$	N [Cycles]	$N_{req.}$ [Cycles]	UF
258	370	0.002352	69,667	60,000	0.86

5. Conclusions

This paper describes a design optimization process carried out on the UM4 mirror that investigates electromagnetic, thermal and structural aspects, seeking for an optimal design solution that withstands a specific (ID 6, [3]) disruptive ITER scenario.

Starting from an existing design, the structural parametric analysis described in §2 investigates on the root cause of the CFP failure, finding that the VDEII EM loads must be reduced by 50 % for a CFP structural integrity compliance to the design code.

A parametric EM transient analysis first shows the cause of the severe magnetic load, investigating on two possible design modifications intended to achieve the 50 % load reduction. The reduction is achieved reducing the surface coverage of the Cu alloy heat sink to an "ax" value of 115 mm.

The USM4 design modification is finally thermo-mechanically verified against the NO scenario showing the compliance with the SDC-IC code.

Additional analyses shall be performed to complete the work package, such as:

- Reconciliation of the USM4 design into the global EM analysis [5] to update and validate the EM load extracted in §3
- Validation of the CFP design using the updated global EM loads.
- Validation of the thermo-mechanical aspects of the USM4 via CFD analyses, updating BCs and therefore validating the upper steering mechanism design.

Declaration of Competing Interest

The authors declare that they have no known competing financial interests or personal relationships that could have appeared to influence the work reported in this paper.

Acknowledgments

This work was carried out within the framework contract OFC-0958. The view and opinions expressed herein do not necessarily reflect those of the European commission of ITER

References

[1] A.M. Sanchez, et al., Design and numerical analyses of the M4 steering mirrors for the ITER Electron cyclotron heating upper launcher, IEEE Trans. Plasma Sci. 47 (12) (2019) 5271–5276.
[2] P. Silva, et al., Design and thermal-structural analyses of ancillary components for the optical steering mirror (M4) for the ITER ECH upper launcher, IEEE Trans. Plasma Sci. (2019) 1525–1530.
[3] Component Load Specification_Upper Launcher In-vessel Mirrors, 2019. F4E_D_2FEY28 v1.7.
[4] N. Casal, EC UL Sub-System Load Specification, F4E_D_25QD28 v5.0, 2021.
[5] P. Testoni, Technical Note on the ECHUL M4 Upper Rotor EM Analysis B2 Vs B3, F4E_D_2KSWLS_v1.0, 2020.
[6] V. Barabash, Appendix A, Material Design Limit Data, ITER_D_222RLN, v3.3, 2013.
[7] V. Barabash, In-vessel Components, SDC-IC, 2021. ITER_D_222RHC v 3.0.
[8] https://www.ansys.com.
[9] S. La Rovere, EC UL PP Updated EM Load Computation Report (Task 5, Option 3), F4E_D_2GCQSQ v1.0, 2019.
[10] A.M. Sanchez, et al., Electromagnetic and mechanical analyses of the ITER electron cyclotron Upper launche steering M4 mirrors for the vertical displacement event, Fusion Eng. Des. (2020) 0920–3796.
[11] M. Vagnoni, Heat Loss on In-vessel Mirrors, F4E_D_29FXNA v1.0, 2017.